Experiments in Fluids 18 (1994) 59–68 © Springer-Verlag 1994

Imaging of premixed flames in microgravity

L. W. Kostiuk, R. K. Cheng

Abstract A laser schlieren system which uses video recording and digital images analysis has been developed and applied successfully to microgravity combustion experiments performed in a drop-tower. The optical system and the experiment are installed within a small package which is subjected to free-fall. The images are recorded on video tape and are digitized and analyzed by a computer-controlled image processor. The experimental results include laminar and turbulent premixed conical flames in microgravity, normal positive gravity (upward), and reverse gravity (downward). The procedures to extract frequency information from the digitized images are described. Many gross features of the effects of gravity on premixed conical flames are found. Flames that ignite easily in normal gravity fail to ignite in microgravity. Buoyancy driven instabilities associated with an interface formed between the hot products and the cold surrounding air is the mechanism through which gravity influences premixed laminar and turbulent flames. In normal gravity, this causes the flame to flicker. In reverse gravity, $-g$, and microgravity, μg, the interface is stable and flame flickering ceases. The flickering frequencies of $+g$ flames vary with changing upstream boundary conditions. The absence of flame flickering in μg suggest that μg flames would be less sensitive to these changes.

1 Introduction

The study of combustion in microgravity (μg) environment contributes to the understanding of many fundamental combustion phenomena as gravity can be a disruptive force. Without buoyancy, hot product gases no longer rises to cause flow asymmetries and instabilities. Flame-flow interactions that are usually overwhelmed by the effects of gravity can be investigated to elucidate the underlying physical and chemical processes. Most early microgravity combustion works have focused on flame spread phenomena to address fire-safety issues in spacecrafts. Since then, microgravity combustion research has been extended to many other areas. Theoretical studies of isolated droplet burning is one area that has benefited from microgravity experiments (e.g., Choi et al., 1992). Other microgravity combustion studies include formation of premixed cellular flame structures (Dunsky, 1991), laminar jet diffusion flames (Bahadori et al., 1990), unsteady flame propagation (Ronney, 1990), flame tip flickering and the polyhedral structure of Bunsen flames (Durox et al., 1990) and our investigation of premixed turbulent flames.

Microgravity experimentation is much more difficult than in normal gravity laboratories because of a variety of operational and physical constraints. These constraints present challenges that are different depending on the facilities used to achieve reduced gravity. Ground-based facilities such as drop towers, parabolic flights, and sounding rockets all have limited duration of reduced gravity. Space experiments offer longer duration and near zero-gravity but flight opportunities are extremely rare. All these facilities require experiments that are operator-independent, self contained, compact, and constructed to withstand vibrations, large rate of deceleration and meet stringent safety standards. Satisfying these requirements have meant that only very simple basic diagnostics can be used. Until recently, movie cameras and thermocouples were the only instrumentation used in microgravity experiments. This can put severe limitations on the kind of information that can be obtained.

The scientific objective of our microgravity combustion research is to investigate the coupling of gravity with laminar and low Reynolds number turbulent premixed flames. Open flames with simple flow geometries have been used extensively for validating numerical and theoretical models. The effects of the far field, i.e., the so-called elliptical problem, which are directly related to buoyancy forces has not been addressed satisfactorily. Our approach is to conduct μg experiments and compare the results to laboratory flame subjected to positive gravity (flames pointing up, $+g$) and reverse gravity (flames pointing down, $-g$). Reconciling the differences in $+g$ $-g$ and μg flames will help to elucidate the coupling between the flame and its flow field. The μg experiments are performed in the 2.2

Received: 2 November 1993/Accepted: 30 June 1994

L. W. Kostiuk[1], R. K. Cheng
Combustion Group, Energy and Environment Division,
Lawrence Berkeley Laboratory,
Berkeley, CA 94720, USA

[1]Present address:
Department of Mechanical Engineering,
University of Alberta,
Edmonton, Alberta T6G 2G8,
Canada

This work is supported by NASA Microgravity Sciences and Applications Divisions under contract No. C-32000-R through the U.S. Department of Energy Contract No. DE-AC03-76F00098. Technical support is provided by NASA Lewis Research Center. Project Scientist is Dr. Karen J. Weiland. The authors would like to acknowledge Dr. Liming Zhou for his contribution to early testing of the schlieren system, and to Mr. Gray Hubbard for writing the image analysis software

second drop tower facility at NASA-Lewis Research Center (LeRC).

In normal gravity laboratory experiments, laser diagnostics with high spatial and/or temporal resolutions are used routinely to interrogate the complex premixed turbulent flame structures (e.g. Cheng and Shepherd, 1991). The types of quantitative statistical data obtainable are in stark contrast to the qualitative information derived from direct photography of flame luminosity. But not all laser diagnostics are readily deployable for microgravity experiments because the optics, laser source, experimental apparatus have to be fitted inside a small experimental package. Moreover, the system has to be sufficiently rigid to withstand the vibrations and impact experience during the course of the microgravity experiments. Our approach is to design a simple premixed flame experiments, and select laser diagnostics that are not very complicated, but have the potential of providing useful information needed to gain insight into the problem to guide our future works. Because the time available for data logging during each ring is only about 2 second, and the number of runs are limited, ease of data collection and monitoring is also a very important consideration.

We have chosen to use laser schlieren coupled with video recording and digital image processing. Adapting laser schlieren to microgravity experiments provided us with the learning experience necessary to adapt other more complex laser diagnostics. Schlieren optics is relatively simple and does not require a high power laser source or very precise alignment. Although it is a so-called 'line-of-sight integration' technique, it will be shown that with the selection of the proper flame configuration to take advantage of the unique feature of premixed flames, quantitative information can be deduced from the schlieren images. The objective of this paper is to present the methodology in applying laser schlieren to microgravity experiments. The engineering approach and considerations in designing the compact apparatus and optimal systems will be described briefly. Also presented are the image analysis methods and typical normal and microgravity results. The difference in the flame behavior and characteristics under normal and microgravity will be discussed. These experiments demonstrate the feasibility of adapting laser diagnostics to drop tower experiments. This suggests that the use of other techniques such as particle tracking and tomography to microgravity works should also be feasible.

2
Experimental methodology

The most distinctive feature of premixed flames is that combustion reactions occur within thin flame surfaces called flamelets. The flamelets are smooth when there is no turbulence in the approach stream, but are wrinkled when subjected to turbulence. Most premixed turbulent flames of practical interest are within the flamelet regime. Because the thickness of the flame surface is close to that of laminar flames, these flames are also known as wrinkeled laminar flames.

The thin flamelets also mean that the flame zone is characterized by large density gradients. This offers high sensitivity to the application of light deflection techniques such as schlieren, deflection mapping and interferometry. A typical flamelet oriented parallel to the incident beam direction (i.e. density gradient orthogonal to beam) creates a deflection, θ, of 10^{-2} radians (Weinberg, 1962). Because schlieren is only sensitive to density gradients orthogonal to the beam, flamelets normal to the beam direction are transparent. For the conical flame configuration chosen for the microgravity experiments, schlieren can outline the flame cone very clearly. This flame configuration has been used in previous microgravity studies of rich propane/air flames (Durox et al., 1990).

We choose video over high speed 16 mm movie camera to be the recording medium. Videos allow for easy monitoring of the experiments and quick review of the results. Moreover, CCD (Charged Coupled Device) video cameras are compact and offer high shutter speed (up to 1/10000 sec) to freeze fast moving flame structures. Although the video framing rate is limited to 30 Hz and may not be sufficient to resolve the evolution of the turbulent flame structures, the benefit of easy monitoring far out-weights this limitation.

3
Experimental apparatus and procedure

The maximum size of the NASA-Lewis 2.2 second drop tower package is 46 cm by 99 cm and 92 cm high. The schlieren system, laser source, camera, burner, flow supply, ignition mechanism, computer controls are fitted on three levels (Fig. 1). The burner is mounted between the two schlieren lenses l_1 and l_2. The optics platform is made of 12 mm aluminum sheet crossed braced for structural stability with 25 mm square bars. Most of the optical rails and mounts are standard commercial items with the stems made very short to minimize movements and bending. The light source is a 5 mw He-Ne laser. No spatial filter was used because its tolerances for alignment were too strict to cope with any slight movements.

To compromise the conflicting requirements of space limitation and sensitivity, the optical lay-out is non-standard with l_1 and l_2 having different focal lengths. The first schlieren lenses, l_1, has a relatively short focal length f_1 of 300 mm to reduce the total path length. The second schlieren lens, l_2, has a longer focal length, f_2, of 1000 mm to enhance the sensitivity (proportional to $f_2\theta$). The system has a 75 mm field of view (i.e. diameters of l_1 and l_2). A 1.5 mm diameter opaque circular schlieren stop was used. It creates a reverse field image because the undeflected beam is blocked and only the regions of density gradients appear bright. The dark background masks imperfection in the optics such as interference patterns inherent from using a laser light source, and non-uniform illumination caused by not having a spatial filter. Another reason for selecting the reverse field configuration is that bright schlieren silhouette against a dark background is easier to enhance by image processing techniques.

The schlieren images are captured by a compact monochromatic CCD camera with a 5% transmittance filter mounted directly onto the camera. A simple 100 mm lens, l_3, is placed in front to form the schlieren image. Mounting the imaging lens, l_3, separately is a more stable arrangement than attaching a standard *C*-mount lens. The larger *C*-mount lens would add extra weight and shift the center of gravity forward. The composite video signal is converted into an optical signal and transmitted by a fiber optic cable to the top of the drop tower and recorded by a S-VHS recorder. The schlieren images are monitored during the drop so that any shift in the optical

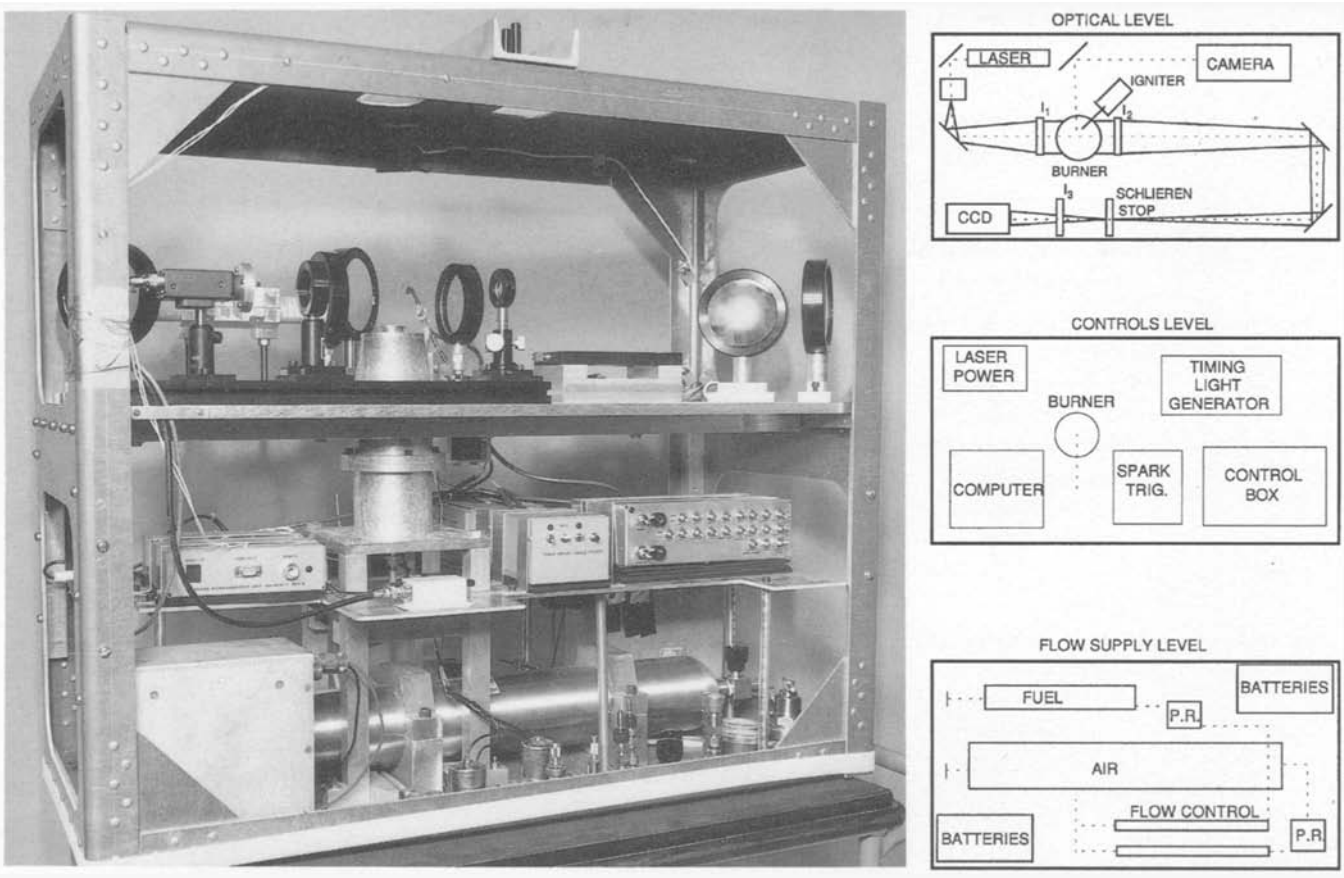

Fig. 1. Schematics of the drop package

alignments or problems with flame ignition can be detected immediately.

Experiments are of lean premixed methane air flames. Fuel and air are stored separately in two stainless steel vessels with pressure regulators and needle valves to control the flow rates. Before each drop, the flow rates are adjusted by calibrated rotometers to a given fuel air ratio and nozzle exit velocity. The two streams are fully premixed in the piping before entering the burner. The burner has a 76.2 mm diameter cylindrical settling chamber and a convergent nozzle which has a 25.4 mm diameter exit. Flow at the exit is uniform and the velocity fluctuations are less than 1%. To produce turbulent flames, a perforated plate with 3.2 mm holes and 50% blockage ratio is used. Since lean premixed flames cannot be stabilized easily on the burner rim, a metal ring mounted at the burner exit is used. The diameter of this ring is slightly smaller than the burner exit. It generates a flow recirculation where the flame anchors. The resulting flame is conical much like a Bunsen flame. The flames are ignited by a spark source which discharges from the ignitor tip to the stabilizer ring. A linkage mechanism driven by solenoid launches and retracts the spark tip.

The microgravity experiments are controlled by an onboard computer. After the package is lifted to the top of the drop tower, the schlieren system and the fiber optics connection are checked by viewing the schlieren images. Final adjustment of the optics can be made and a recording of the normal gravity flame is also obtained as a reference. Seven seconds before releasing the drop package, the fuel and air valves are opened to purge the burner of residual air. When the package is released, an electrical connection is broken to start the program which triggers the spark ignitor after a 0.1 seconds delay.

4
Image processing and analysis

The image processing and analysis procedure is shown schematically in Fig. 2. Typically, two seconds or 60 frames of data from each experiment are digitized. For this analysis, the time sequence is important so the video images must be digitized and stored in order. Two methods of digitizing the videos were used. The first is a computer based frame grabber and animation controller interfaced with the video editor (Johnson et al. (1990)). This system uses the time code information written on the linear audio track of the video tape as the frame markers. The digitized monochrome images have 512×512 pixel resolution with 8 bit deep intensity mapping. The process is relative slow. The Abekas based editing facility at LeRC is five hundred times faster. This is a color system and therefore requires further processing of the digitized images to turn them into monochromatic.

Each full video frame consists of an odd and an even field that are interlaced (i.e., stored on alternate horizontal lines)[1]. These

[1]This is the reason why horizontal strips flicker when shown on TV. Most VCRs show composite interlaced freeze-frame images. Some S-VHS and Hi-8 equipment show individual fields at freeze frame and have the capability of showing each field sequentially in slow-motion

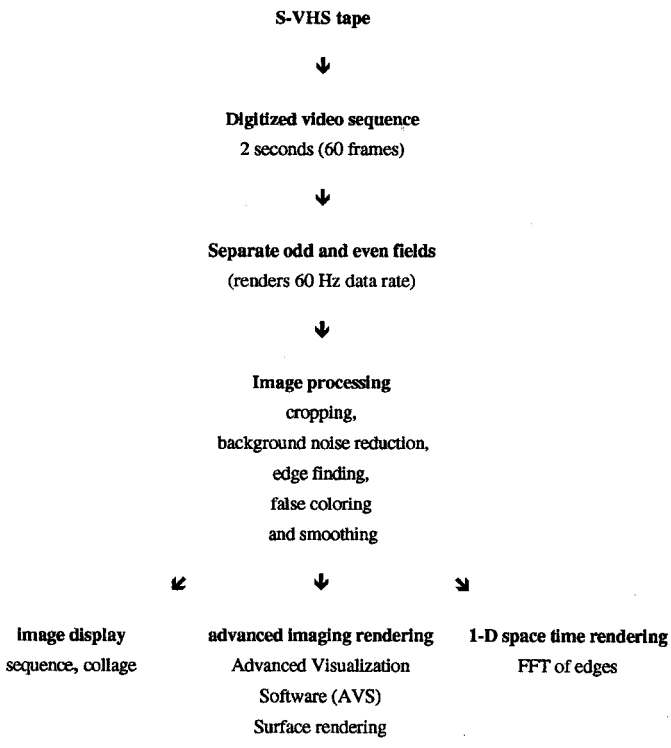

Fig. 2. Image processing flow-chart

Fig. 3. Schlieren image of a $+g$ laminar methane/air flame with flow rate of 0.42 lire/sec and $\phi = 0.9$

individual fields are not captured at the same instant but at 1/60 seconds apart. Though this video feature is relatively well-known, it is seldom exploited in scientific experiments to obtain time information. For high shutter speed recording such as ours, the effectively framing rate is actually 60 Hz. To render the sequential 60 Hz data, each image is separated into two odd and even images of 512 by 256 pixel resolution. 120 field images from 2 seconds of video tape are obtained from each experiment.

The digitized images are processed by several standard techniques as listed in Fig. 2. In addition to displaying them in time sequences, different rendering methods can be used to bring out the small changes and evolution of the flame structures. Some quantitative time scales information can also be deduced. These results can be compared with those of the flow and flame structures.

5 Results

5.1 Schlieren images

The experimental conditions investigated in normal and microgravity range from flow rate, $\dot{m}$, of 0.2 to 0.9 liter/sec (mean centerline velocity of 0.5 to 2.0 m/s), and methane-air equivalence ratio, ϕ, from 0.65 to 1.0. In addition to schlieren videos, LDA measurement of the $+g$ and $-g$ flames obtained in our laboratory provide the necessary background information to guide the interpretation of the μg schlieren results. Twenty-one successful microgravity experiments have been completed during two visits to the drop tower at LeRC. The μg experimental conditions consisted of five laminar flames and three turbulent flames. These are the first successful applications of laser schlieren to drop tower experiments and the first investigation of open premixed turbulent flames in microgravity.

Clearly, the major concerns prior to the first drop were whether or not the optics would remain aligned during the drop and if extensive realignment would be necessary afterwards. Fortunately, the optics remained relatively stable during the experiments. However, slight optical mis-alignement was not totally avoidable. This causes a semi-circular shadow of the schlieren lens to appear because of the laser beam shifting away from the center of the schlieren stop. After the impact, it was discovered that only one or two optical components were rotated out of axis. Most components exhibited very little or no movement. The schlieren optics could be checked and readjusted quickly. Alignment of the optics therefore does not limit the turn-around time.

Our original plan was to ignite the flame before the release. Under lean conditions, however, the vibrations generated during the release were found to be sufficiently violent to extinguish the flame. Ignition in microgravity circumvented this problem though it reduced the total data time from 2.2 to about 2.0 seconds. We also found that lean flames are more difficult to ignite in microgravity and the problem is more serious for lean turbulent flames. This seems to indicate that the ignition limits is affected by the lack of buoyancy. This interesting flame behavior in microgravity would be a suitable subject for future experiments.

Many characteristics of the Bunsen flames are shown by the schlieren videos obtained for $+g$, $-g$ and μg. VCRs are particularly useful for reviewing the flame flickering phenomenon, the evolution of the flame wrinkles and changes in complex turbulent flame structures. Figure 3 shows a schlieren image of a laminar $+g$ flame ($\dot{m} = 0.42$ l/s, $\phi = 0.9$). The flame cone is seen at the center. The slightly bulging

features on both sides of the flame cone is an unstable interface formed between the hot products and cold room air. This interface is visible only on schlieren images but is absent from flame luminosity photographs.

Time sequences (1/60 sec. between frames) of the schlieren images for the $+g$, $-g$ and μg flames are compared in Fig. 4. For the $+g$ flame, the evolution of the buoyancy driven product/air interface is clearly shown. The small movements of the flame tip that are obvious when viewing the video direct, are not easily discernible from the still image sequence. The flame tip movement, commonly known as flame flickering are synchronized with the pulsating motion of the unstable interface. As shall be discussed later, the pulsating motion has a profound effect on the entire flame flowfield. Under reverse gravity (middle role) buoyancy forces the products to rise and the product-air interface forms a more stable envelop covering the flame cone from below. The flame tip ceases to flicker but some intermittent wrinkling of the flame is shown. Under low flow rate conditions, ($\dot{m} \approx 0.2$ liter/sec) the buoyancy products can flatten the flame tip and form a locally horizontal flat flame region below the burner center. For the μg case, the hot products do not rise but move outward into the surrounding air and maintain a quasi-steady state. The density gradient of the interface in μg is much weaker and it is almost invisible. The circular patch seen at the upper right side of the flame tip is the only remaining feature. The semi-circular arch below the flame cone is just the shadow of the schlieren lens due to a slight shift in the schlieren alignment. Without the influence of buoyancy driven instability, the μg flames are much more stable than the $+g$ flames. Under conditions of low flow rate, a slight flattening of the μg flame tip is observed occasionally. This is similar but far less severe than that observed in $-g$ flames. These schlieren videos clearly show the coupling of premixed flames with the gravity field and confirm that buoyancy driven instabilities is the dominant cause of the flame flame flickering phenomenon of premixed flames.

Schlieren sequences of $+g$ and μg turbulent flames (Fig. 5) show the characteristic wrinkled structures of turbulent flame with low turbulence intensities. For the $+g$ case, the outer unstable product/air interface is again visible and evolves in a manner similar to that observed in laminar flames. Flame flickering in synchronous with the pulsating interface motion is easier to discern here. For example, flame height shown in the third frame from the left is significant shorter than that shown

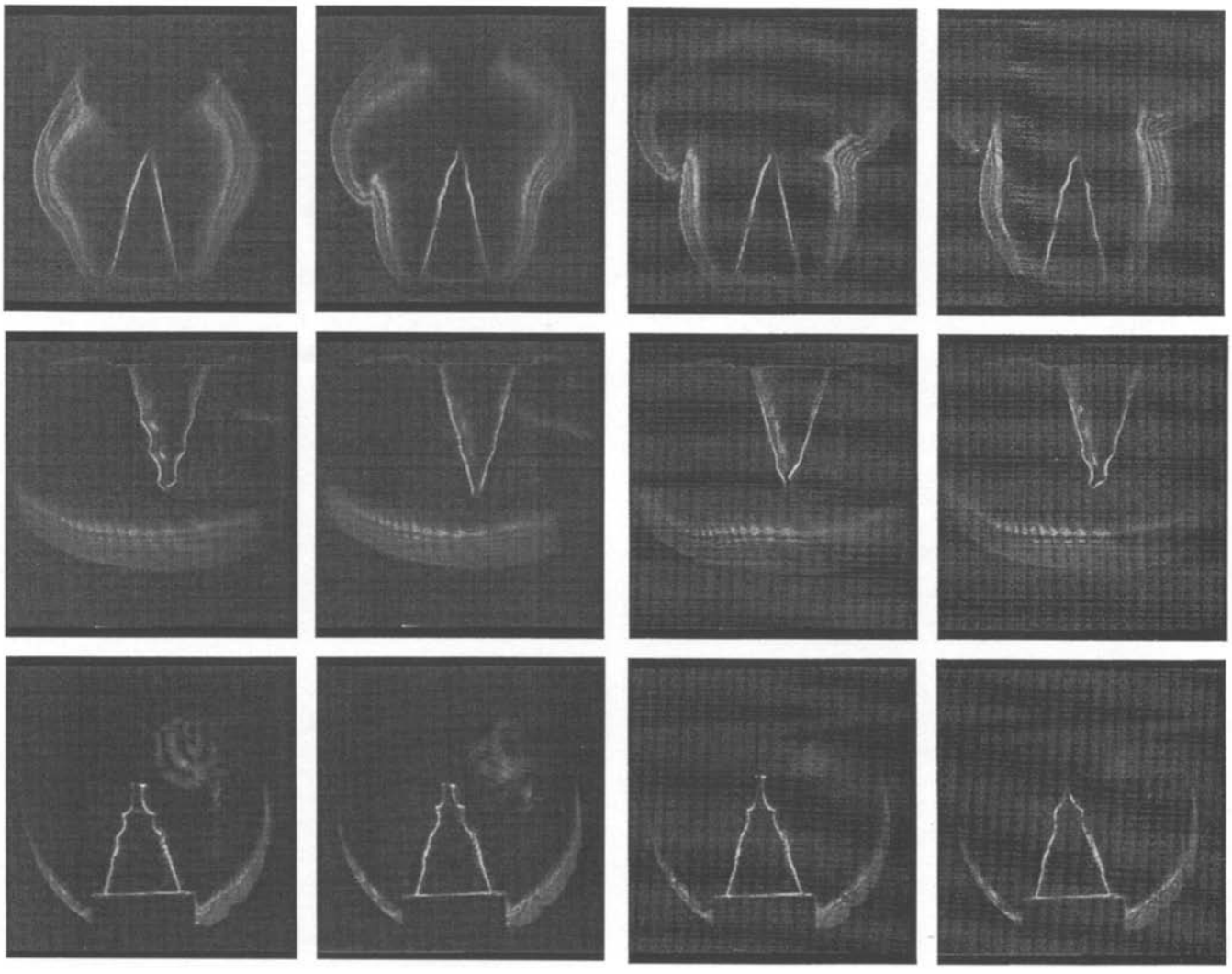

Fig. 4. Sequences of imaged obtained for the $+g$ (top) $-g$ (middle) and μg (bottom) laminar flame with $\phi = 0.9$ and flow rate of 0.42 lire/sec

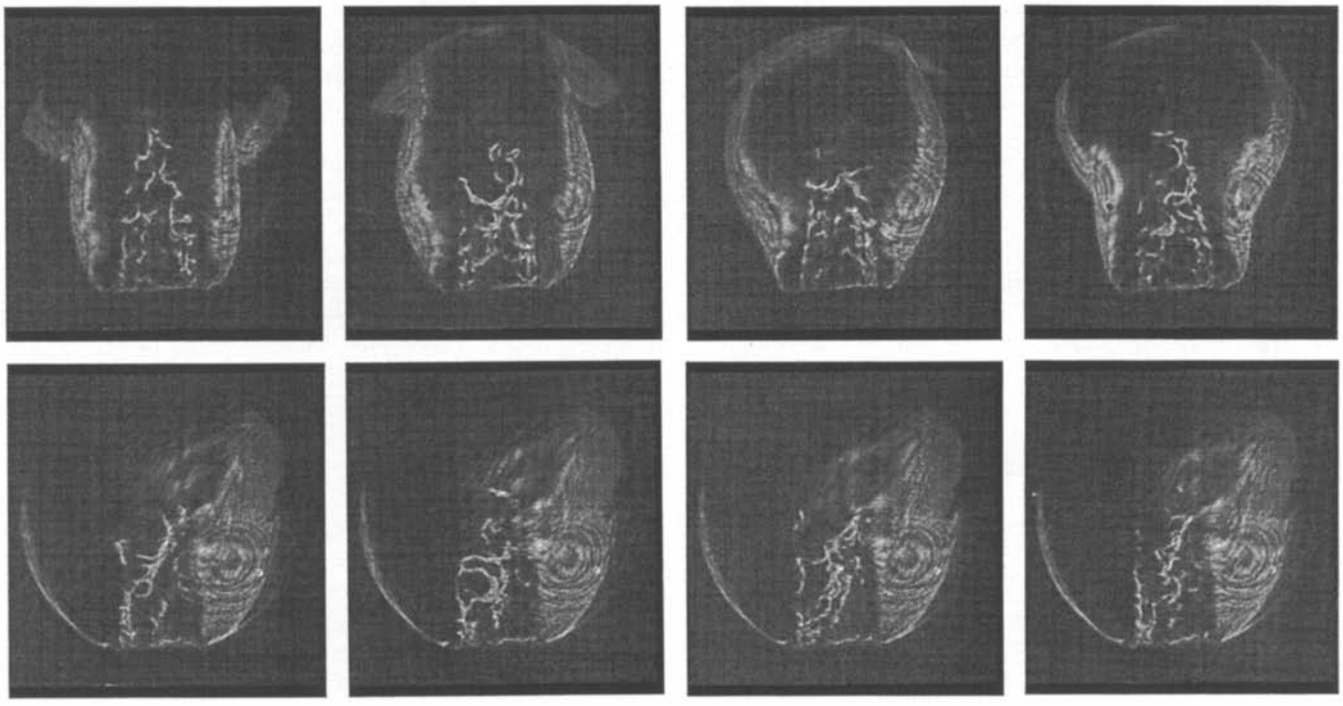

Fig. 5. Sequences of images obtained for the $+g$ (top) and μg (bottom turbulent flame with $\phi = 0.75$ and flow rate of 0.42 lire/sec

on the first frame. Under μg, the product/air interface is still visible to the right of the flame cone and it ceases to pulsate. There is no change in the shape of the interface shown on the four consecutive frames. Because of a shift in the schlieren alignment, the image of the interface partially obscures the turbulent flame. In contrast to the laminar product/air interface which becomes only barely visible in microgravity, the interfaces of turbulent flames are always seen on the schlieren images. This suggests a higher density gradient across the interface for the turbulent cases. The two factors which may account for this difference are the higher turbulent flow rates and the presence of turbulence in the hot products. The video shows that the interface has some small perturbations in μg.

Because turbulence fluctuations occur at the time scale much smaller than the 60 Hz video rate, the only time information that can be deduced for the turbulent flames is the pulsating frequency of the $+g$ flames. Temporal or spatial analysis of the disjointed wrinkled flame structures is not expected to produce very meaningful results. However, time mean properties of the flame brush (e.g., mean flame height and thickness) can still be determined for comparison between $+g$ and μg cases. This can be done by summing all the images and producing an iso-intensity contours of the composite. Even though video recording is not sufficient to resolve the evolution of the wrinkled flame structures, these results have clearly shown that the product-air interface is the mechanism through which gravity influence premixed laminar and turbulent flames.

5.2 Image analysis

The main drawback in presenting the schlieren video as still images is that the changes shown vividly on the videos are not easily conveyed. We have tested several advanced rendering methods but none of them was found to be satisfactory. One method was to display the images in a 3-D array with time being the third dimension. The iso-intensity surfaces in the 3-D domain can be smoothed and displayed at different angles of rotation. This method was found not to be effective because it introduces artificial features that are quite distracting. A simple display we have found is to place a time sequence of cropped images adjacent to each other. This allows the evolution of the flame or interface features to be followed. Figure 6 shows the evolution of the product-air interface and the flame cone for the $+g$ laminar premixed flame. The unstable pulsating nature of the interface and the lengthening and shortening of the flame tip can be followed more easily.

Line representation is a convenient and useful method for both displaying and analyzing the schlieren sequences. For laminar flames, both the broad schlieren silhouettes of the product/air interface and the flame cone can be reduced to a single pixel lines. For turbulent flame, the only meaningful line representation would be the unstable interface for the $+g$ flames. The line representations are extracted by an edge detection routine. The most consistent method we have found is based on locating the outer edges of all of the schlieren silhouettes. The algorithm scans each horizontal pixel line from both the left and the right. The edges are defined by the pixel locations with light intensity exceeding a fixed threshold. The outer edges have sharp intensity gradients and the positions of the line representations are not sensitive to the choice of the threshold. Figure 7 shows the results obtained for the image of Fig. 3. The essential features of the flame and product/air interface are well preserved. Problems only arise when complex structures is encountered. This is evidence for the rolled-up product interface near the top left corner.

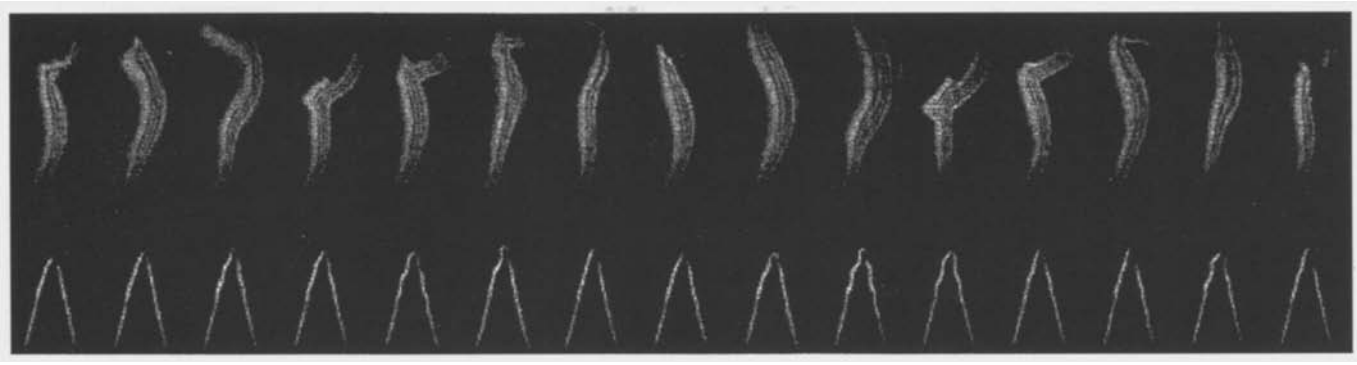

Fig. 6. Cropped images showing the evolution of product/air interface and the flame tip. The pulsating nature of the interface is clearly shown. The flame tip movement is harder to discern

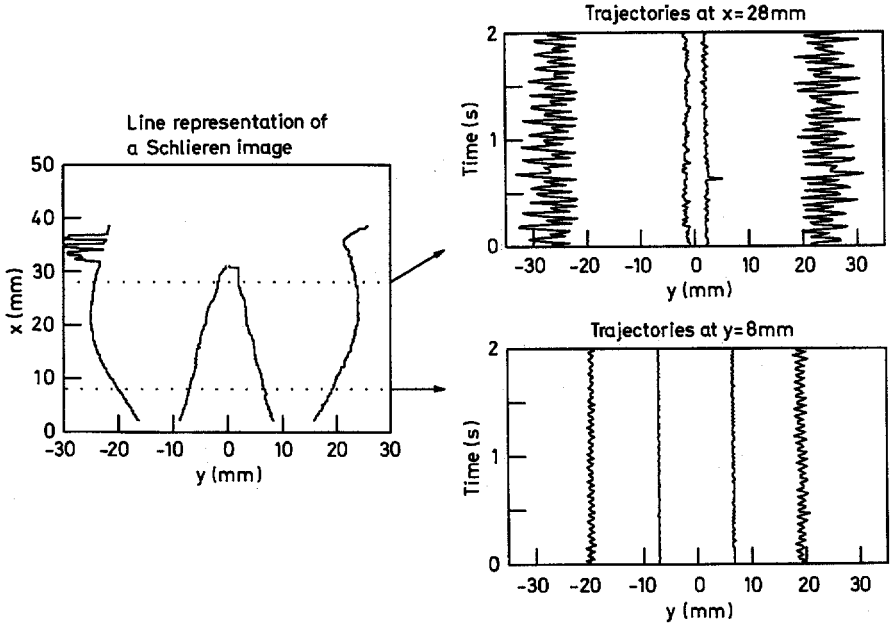

Fig. 7. Line representation of the schlieren image shown in Fig. 3c. The trajectories of the lines at two heights, 18 mm and 28 mm, are shown to the right

The data set containing 120 frames of the four line representations are transformed to space-time trajectories to extract time information. Shown to the right of Fig. 7 are two sets of trajectories at 8 and 28 mm above the burner exit. The outer and inner trajectories correspond respectively to the two sides of the product/air interface and the flame cone. The large fluctuation amplitude and the regular pulsating nature of the product/air interface are obvious at $x = 28$ mm. The high cross correlation coefficient (> 0.9) between for the two sides of the product/air interfaces shows that a vortex ring is formed. The pulsation of the interface is evident even at $y = 8$ mm where the fluctuation amplitude is much smaller. In contrast, the intensity of the flame movement is much smaller. The fluctuations shown at $x = 8$ mm are essentially digitization noise. Near the flame tip, at $x = 28$ mm, flame fluctuation is larger, the rms value at this position is about 0.6 mm. The cross correlation coefficients of the flame trajectories with the product/air interface trajectories are less than 0.5. The reason for this relatively low value is because the gross flame motion associated with flickering is in the vertical direction. Never-the-less, the cross-correlation demonstrate the synchronous movements of the products/air interface and the flame.

5.3
Flame flickering and far-field effects

Flame flickering is a well known flame instability problem. Our schlieren investigation has shown that it is a direct result of buoyancy and microgravity flames cease to flicker. Therefore, understanding flame flickering phenomenon and the parameters that control its frequency would be very useful for our further studies of the behaviour of microgravity flames. However, theoretical analyses of flame flickering are developed mostly for diffusion flames. The well-known "infinite candle" diffusion flame model of Buckmaster and Peters (1986) has shown the relationship between flame flickering and buoyancy. It explains why the flame flickering frequencies tend to be invariant. Because this analysis does not account for the effects of flow momentum, it is not appropriate for explaining the flickering of premixed flames. Durox et al. (1990) observed flame flickering of rich conical laminar flames under enhanced gravity and microgravity conditions. They reported increases in flame flickering frequencies with flow velocity. Without the benefit of schlieren imaging which shows clearly the coupling between flame tip movement and the pulsating interface, they proposed an explanation that relates flickering to flame front instabilities.

From the schlieren images, the flame flickering frequency can be extracted by performing Fast Fourier Transform (FFT) of the trajectories at any given horizontal position. The spectra obtained by FFT for the right interface of the laminar flame in Fig. 7 are shown in Fig. 8. The middle and bottom spectra are deduced from the trajectories at $x=28$ and 18 mm above the burner exit. Due to the strong regular pulsating motion, a peak at 16 Hz and its sub harmonic frequency at 8 Hz are shown. The sub-harmonic peak is more pronounced on the top spectrum obtained from summing all the trajectories from $y=10$ to 40 mm. This is justified because phase information is not concerned. The noise on this spectra is less than those of the other two. The maximum peak at 16 Hz is in accord with the flame flickering frequencies reported by Durox et al., (1990). Spectral analysis is also performed on the flame trajectories. Figure 9 shows three spectra obtained at two positions and the one deduced from summing the trajectories near the flame tip. Despite the fact that the fluctuation intensities are small, a small peak near 16 Hz is a consistent feature of all three spectra. It is then clear that the pulsating motion of the product-air interface is the cause of laminar flame flickering.

The pulsating motion of the interface has a far-reaching affects throughout the entire flame flowfield. It induces velocity fluctuations within the reactants upstream of the flame cone. Figure 10 shows velocity spectra measured by LDA in the reactants, flame zone and products of a $+g$ laminar flame ($\dot{m}=0.51$ l/s, $\phi=0.9$). These spectra are characterized by a single peak at 18 Hz. Even though the fluctuation intensity in the reactants is almost two orders of magnitude lower than in the flame zone, all the fluctuation energy are contained in that peak. Without the flame, the flow issuing from the burner is laminar and the spectrum is flat. The effects of the pulsating interface on the turbulent flame flowfield is just as pronounced. Shown in Fig. 11 are spectra obtained for a $+g$ turbulent flame ($\dot{m}=0.55$ l/s, $\phi=0.7$). They are also characterized by a single peak at a higher 18 Hz. Above this peak frequency, the spectral distributions are all typical of turbulence generated by grid or perforated plates. The flickering frequencies of the laminar and turbulent flames are the same. Therefore, turbulence transport has no effect on the flickering phenomenon. These results together with the flickering frequency deduced for the flame shown in Fig. 3 demonstrate that the flickering frequency increases with flow rate. This is in accord with the observations of Durox et al. (1990).

From watching the development of the pulsating interface on video, it appears that a consequence of the pulsating interface is to entrain still air into the products. This entrainment process would induce air motion in the surrounding region. Therefore, changing the upstream boundary conditions could alter the entrainment process and may in turn affect flame flickering. To test this hypothesis, we changed the upstream boundary conditions of a laminar flame by fitting circular plate collars of increasing diameters, D, to the burner exit. Without the collars, the burner exit ($d=2.54$ cm), is actually located at the center of

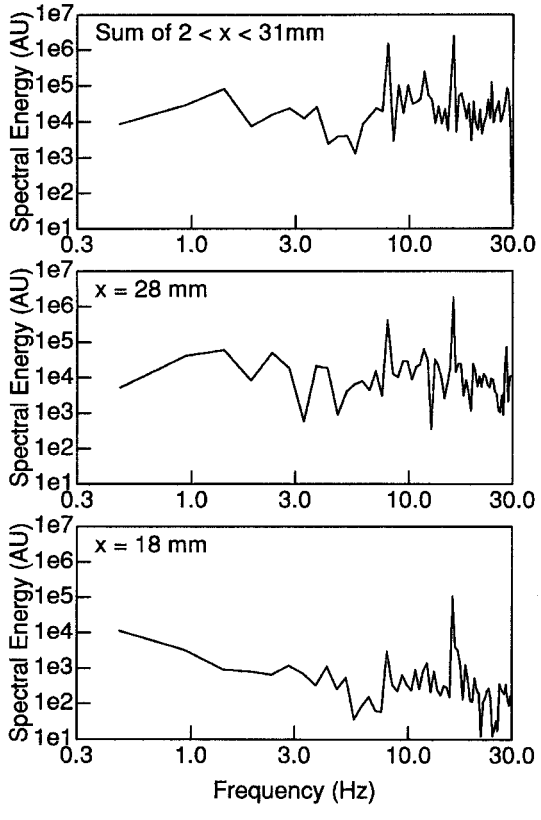

Fig. 8. Spectra deduced from the right product/air interface trajectories of Fig. 7

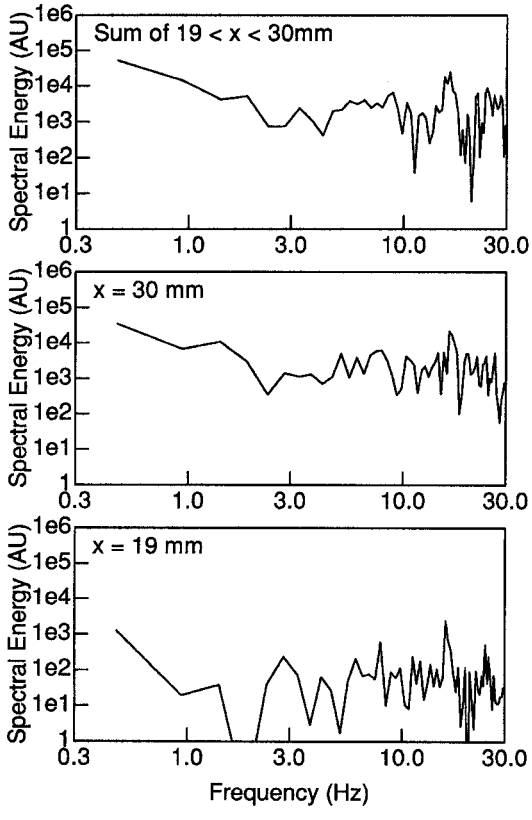

Fig. 9. Spectra deduced from the right flame trajectories of Fig. 7

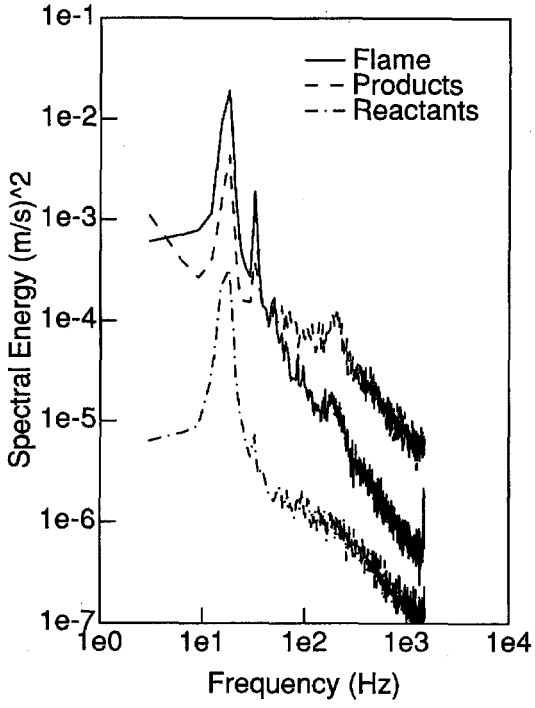

Fig. 10. Velocity spectra measured in three regions of a laminar flame with flow rate of 0.54 and $\phi = 0.9$

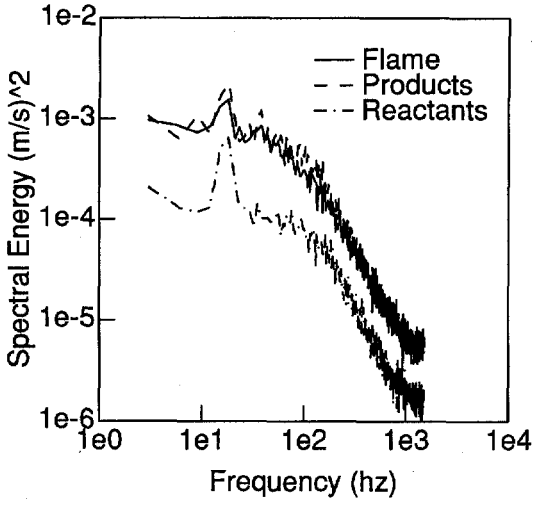

Fig. 11. Velocity spectra measured in three regions of a turbulent flame with flow rate of 0.54 and $\phi = 0.7$

a larger round 7.62 cm diameter platform. This baseline condition is considered as having a collar to burner diameter ratio, D/d, equals 3.

Figure 11 shows the velocity spectra measured in a flame with $\dot{m} = 0.45$ l/s and $\phi = 0.9$ with D/d increasing from 3 to 7. The spectra are presented in a log-linear plot to better illustrate the shift in the dominant frequency and the reduction in spectral energy. Without the collar ($D/d = 3$) the dominant fluctuation frequency is 16 Hz. With increasing D/d, the dominant frequency shifts to lower values and the peak spectral energy is also reduced. At $D/d = 7$ and beyond, no dominant frequency is

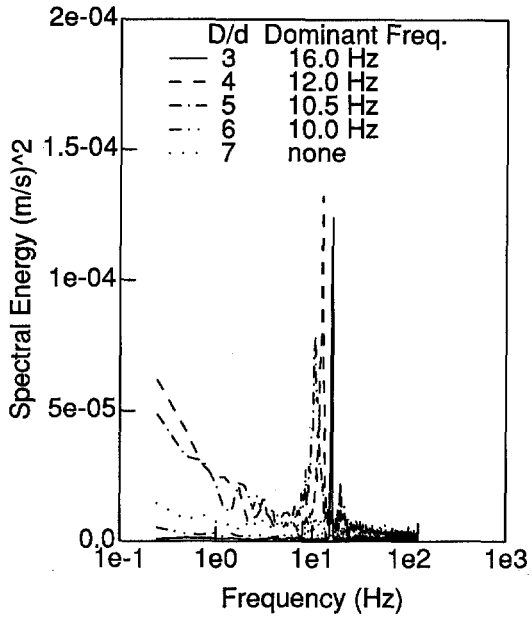

Fig. 12. Flickering frequencies of a laminar flame with changing upstream boundary conditions

found. The companion schlieren videos show that with increasing D/d the amplitude of the interface motion also decreases. These results clearly demonstrate the elliptical nature of the flame flowfield. Theoretical treatment of buoyancy driven premixed flame instabilities would be incomplete without considering the far-field boundary condition effects. These results also imply that without the entrainment process associated with the pulsating interface, microgravity flames would be less sensitive to changes in the upstream conditions. We plan to address this interesting issue and other microgravity flame phenomenon in our future microgravity experiments.

6 Conclusions

Our study has shown that laser schlieren can be used successfully in drop tower experiments. The optical system is sufficiently rigid to withstand the impact forces at the end of the drop. Realignment of the optics does not present a rate limiting step in the experimental process. Therefore, other laser diagnostic can also be adapted if the space restrictions and the effects of bottom impact can be addressed. The convenience of video recording facilitate the experimental procedures and image analysis. The schlieren video are digitized and analyzed to obtain temporal and spatial information.

Taking advantage of the interlaced feature of video recording, an effective framing rate of 60 Hz is rendered. The best means to analyze the schlieren data is to extract line representations of the schlieren silhouettes from which mean, rms, cross-correlation coefficients and spectra are deduced.

Many gross features of the effects of gravity on premixed conical flames are found. Flames that ignite easily in normal gravity fail to ignite in microgravity. The schlieren results clearly show that buoyancy driven instabilities associated with an interface formed between the hot products and the cold

surrounding air is the mechanism through which gravity influences premixed laminar and turbulent flames. In normal gravity, the pulsating nature of this interface causes the flame to flicker. In reverse gravity, $-g$, and microgravity, μg, the interface is stable and flame flickering ceases.

The flame flickering frequencies are deduced by FFT from digitized schlieren images. These frequencies increase with flow rate from 16 Hz to 18 Hz. The unstable interface affects the entire flame flow-field and tends to entrain ambient air into the products. Velocity spectra measured upstream of the flame tip show distinct frequency peaks at the flame flickering frequency. The flickering frequency also changes with different upstream boundary conditions. The changes occur because the different boundary conditions affects their entrainment process. The flame flickering frequency can be reduced from 18 Hz to 10 Hz. These results suggest that microgravity flames are less sensitive to upstream boundary conditions because they do not induced entrainment.

References

Bahadori MY; Edelman RB; Stocker DP; Olson SL (1990) Ignition andbehavior of laminar gas-jet diffusion flames in microgravity. AIAA J 28: 236–244

Bray KNC; Libby PA; Moss JB (1985) Unified modeling approach for premixed turbulent combustion – Part I: General formulation. Combustion and Flame 61: 87–102

Buckmaster J; Peters N (1986) Infinite candle and its stability – a paradigm for flickering diffusion flame. 21st Symp. (Int'l) on Combustion, The Combustion Institute, p. 1829–1836

Cheng RK; Shepherd IG (1991) The influence of flame geometry on premixed turbulent flame propagation. Combustion and Flame 85: 7–26

Cheng RK; Ng TT (1983) Velocity Statistics in Premixed Turbulent Flames. Combustion and Flame 52: 185

Choi MY; Dryer FL; Card JM; Williams FA; Haggard JB; Borowski BA (1992) Microgravity combustion of isolated *n*-decane and *n*-heptane droplets. AIAA Paper No. 92-242

Dunksy CM (1991) Experimental study of the effects of gravity on the stability of premixed laminar flames. Ph.D. Dissertation, University of California, Berkeley

Durox D; Baillot B; Scoufflaire P; Prud'homme R (1990) Some effects of gravity on the behavior of premixed flames. Combustion and Flame 82: 66–74

Johnson WE; Robertson D; Tiernay BL (1990) Acquisition of digital images from video tape pattern recognition and image processing in physics. Scottish Universities Summer School in Physics & Adam Hilger, Bristol, Philadelphia and New York 273–282

Ronney PD (1990) Near-limit flame structures at low Lewis number. Combustion and Flame 82: 1–14

Winberg FJ (1962) Optics of Flames, Butterworth